Fan Noise 2007

CONCEPT, DESIGN AND CHARACTERIZATION OF A SMALL AEROACOUSTIC WIND TUNNEL FACILITY WITH APPLICATION TO FAN BLADE MEASUREMENTS

Julian WINKLER, Fatma Zeynep TEMEL, Thomas CAROLUS

Universität Siegen, Institut für Fluid- und Thermodynamik,
Paul-Bonatz-Str. 9-11, 57068 Siegen, GERMANY

SUMMARY

Experimental investigation of flow-induced sound and sources of sound necessitates an adequate environment of low interfering noise and suppression of unwanted sources of sound. In order to investigate the sound from fluid-structure interactions, a low-noise wind tunnel has been designed and implemented. This paper gives an overview of the design criteria and specifications, along with an aeroacoustic and aerodynamic characterization of the facility. The suitability to airfoil self-noise studies is explored and first measurements with a model airfoil are presented. The paper concludes with suggestions for improvements and provides an outlook on future applications.

CONCEPT AND DESIGN OF THE WIND TUNNEL

Design Specifications

A new small low-speed wind tunnel facility for aeroacoustic research has been designed and built in the Institut für Fluid- und Thermodynamik of the University of Siegen. The following operating conditions have been specified as desirable: The nozzle flow should have a uniform velocity distribution with $\overline{u}_{\max} = 30\,\frac{m}{s}$ and a *local* turbulence intensity $TI = \sqrt{\langle u'^2 \rangle} \,/\, \langle u \rangle < 0.1\%$ in the exit-plane, based on a square nozzle of dimension 133×133 mm^2 ($\langle \ldots \rangle$ denotes time-averaging at a given location and therefore describes local quantities; the overbar denotes space-averaging over the described domain). The facility needs to be *flexible*, i.e. it is desired to have building-blocks that allow for a quick disassembly of the facility, since the anechoic room in which the wind tunnel terminates is also used by other test facilities. To leave room for improvements, the facility should be extendable to a certain degree and building parts should be easily interchangeable.

Three different design configurations have initially been proposed [1], with the main difference being the choice of the muffler(s). For each design, the necessary parts and part dimensions have been selected, based on existing in-house knowledge and extensive literature reviewing. Pressure losses in the facility have been calculated to determine the appropriate driving fan. The final (and selected) design of the facility is presented here, including a description of the incorporated parts. This design was mainly guided by similar wind tunnels at the University of Notre Dame [2, 3] and the Technical University of Dresden [4]. Figure 1 shows a schematic of the wind tunnel facility. Two important flexible design criteria are present. First, the conception of the wind tunnel allows the implementation

of additional screens because the required elements are incorporated as building-blocks. In the same way, screens can easily be removed or exchanged. Second, sufficient space is available between the exit of the muffler and the entrance of the first elbow pipe of the S-shaped bend, to allow for the implementation of an additional splitter silencer, if required. We now describe the components of the facility which have been labeled in Figure 1.

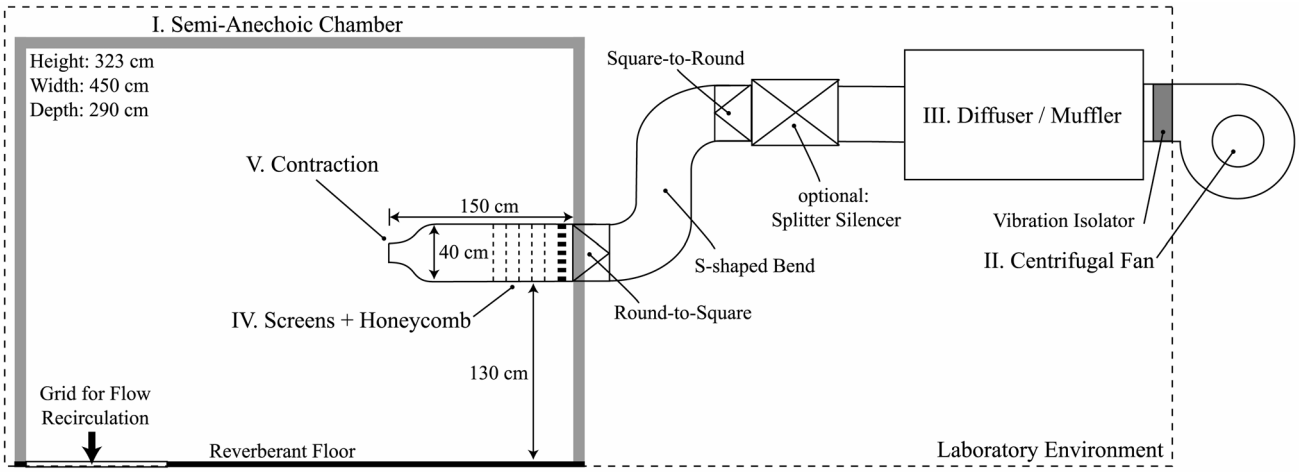

Figure 1: The new aeroacoustic wind tunnel facility (schematically, not to scale)

I. The Semi-Anechoic Chamber

The semi-anechoic chamber is lined with composite slab resonators, developed at the FRAUNHOFER INSTITUTE FOR BUILDING PHYSICS ([5], patent pending). These resonators are composed of two melamine resin foam slabs, 100 *mm* and 150 *mm* thick, partially separated by 1 *mm* steel sheets. The sheets absorb low frequencies at 50 – 100 *Hz* most effectively and reduce the required thickness of the foam slabs. The room has a low cut-off frequency of 125 *Hz*, the background noise level is 33 *dB* (overall sound pressure level, OASPL, in the frequency range 125 $Hz < f < 12.8$ *kHz)*. Flow may recirculate through an opening in the reverberant floor covered by a grid. The chamber's acoustic properties allow acoustic measurements according to ISO 3745 [6].

II. The Drive System

The wind tunnel is driven by a ZIEHL-ABEGG centrifugal fan (type RG50T) with a variable frequency drive (YASKAWA Varispeed F7). The fan works at a maximum rotational speed of 1,395 min^{-1}. It was selected to achieve the desired flow rate ($\dot{V} = 0.54\ m^3/s$), which yields a projected velocity of $\overline{u} = 30\,\frac{m}{s}$ at the nozzle exit (small nozzle, see section V. below) and to compensate for the cumulative (estimated) pressure losses ($\Delta p_{loss} \approx 730\ Pa$) in the facility. The fan is located outside the laboratory environment and is decoupled from the muffler by a square elastic rubber channel-section to avoid transmission of solid body vibrations.

III. The Muffler Design

A muffler-diffuser combination is used, as shown in Figure 2. Our design has been strongly influenced by the specifications of the round cross-section muffler at the University of Notre Dame [2, 3]. The diffuser serves to gradually recover the static pressure from the fan flow. As evident from Figure 2, there is a fourfold increase of the cross-sectional area from inlet to outlet. From the cross-sectional view, it can also be seen that the flow paths are surrounded by a kernel and a blanket of fiberglass ($\rho = 50\ kg/m^3$), which attenuate sound waves through absorption. The walls of the four flow channels consist of perforated sheet metal, with a transparency index

$TPI = 0.04(1-\sigma)/\pi ta^2 = 14{,}187$ (σ is the metal's solidity, i.e. closed to total area in %, t is the thickness of the sheet and a the distance between the holes), which makes the surface acoustically transparent, according to [2, 3]. The sheet metal is covered with glass silk (50 g/m^2) to avoid contamination of the flow by fiberglass. The inclination and the declination of the flow channels support a further attenuation of sound. These types of mufflers are widely used in aeroacoustic wind tunnels.

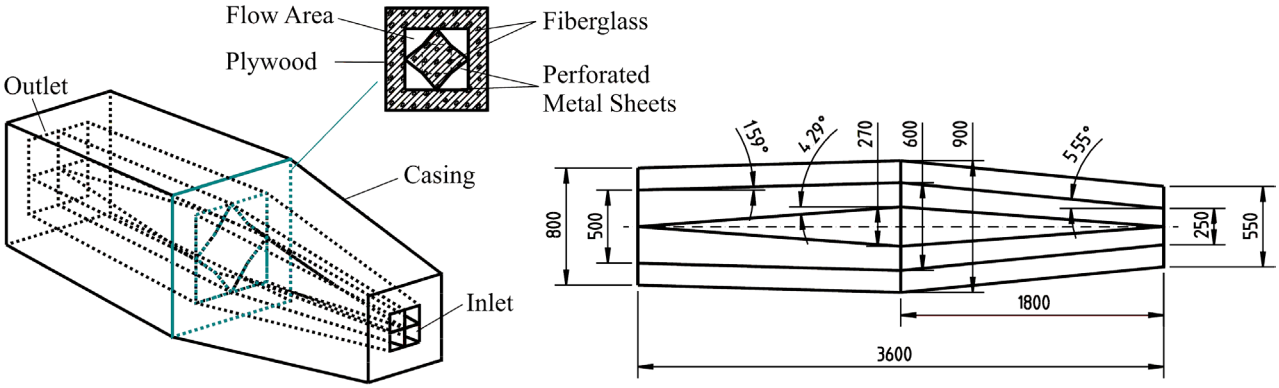

Figure 2: Design of the muffler-diffuser combination

IV. Flow Rectification and Turbulence Reduction

A selection of five screens and one honeycomb is used for rectification of the flow and reduction of velocity fluctuations. The amount of required screens and honeycombs, the dimensions, the location, and the spacing between them, have been selected based on a literature survey. The following recommendations have been adopted: The reduction in axial and lateral turbulence by screens has been calculated from WIEGHARDT's equation (see [7]), from which the number of required screens is determined. The effectiveness of the screen is essentially determined by two parameters: the Reynolds number Re_d based on the wire diameter, and the solidity σ, i.e. the ratio of solid area to total area. The dimensions of the screens should coincide with the restriction that $\sigma < 50\%$ and $Re_d > 40$ (*supercritical*). For lower solidities, instabilities can occur due to jet coalescence [8]. For lower REYNOLDS numbers (*subcritical* screens), turbulence reduction is increased, with the penalty of a higher pressure drop. An arrangement of multiple supercritical screens is found to be superior to a single subcritical screen [8] and more practical (far less susceptible to dirt). The selected screens have a solidity of $\sigma = 0.44$, with a wire diameter of $d = 1$ *mm* ($Re_d \approx 222$) and a mesh size of $M = 3$ *mm*. GROTH and JOHANSSON [8] have shown that directly downstream of the screen turbulence is increased due to vortex shedding from the wires and shear layer presence from the wire wakes. However, the turbulence decays rapidly and at $>20M$ downstream reaches an isotropic state. The screen separation should therefore be larger than this initial decay region. Accordingly, the spacing between the screens (100 *mm*) was chosen to be $\approx 33M$. The honeycomb has a cell size of $H = 5$ *mm* and a depth of $L = 30$ *mm*, which is in accordance to the recommendation by MEHTA and BRADSHAW [7] ($L/H = 6\ldots8$). The distance between the first screen and the honeycomb is $<5C$ [9].

V. Contraction

The aim of the contraction is to produce a uniform flow of low turbulence intensity [10]. Some critical design parameters are the relative contraction length L/D_1, the contraction ratio A_1/A_0 and the contour $D(x)$ [11], where "1" denotes the inlet plane and index "0" the exit plane. In general, the contraction should be as short as possible to limit extensive boundary layer growth. Yet, the contraction ratio should not be too high, to prevent boundary layer separation associated with the

adverse pressure gradient occurring at high curvature. Two interchangeable square nozzles have been manufactured with exit-plane dimensions of 133×133 mm^2 and 180×180 mm^2, i.e. contraction ratios of 9 and 4.9 with relative contraction lengths of 0.75 and 0.82, respectively. The chosen nozzle contour is of minimum curvature; it is described by two intertwining radii which meet at the matching point, located in the middle between nozzle entrance and exit. Figure 3 shows a scheme of the nozzle, along with the implemented final design. The actual nozzle exit-side (at D_0) is extended by $\Delta x = 0.075 D_1$ in length to obtain smoother exit conditions for the flow.

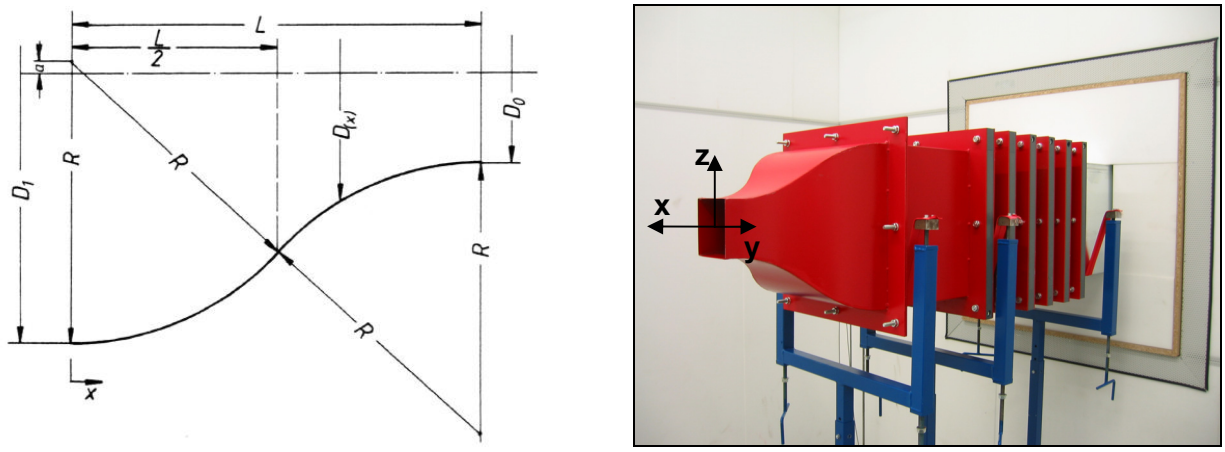

Figure 3: Nozzle contour (left) and final assembly with coordinates (right)

AEROACOUSTIC AND AERODYNAMIC CHARACTERIZATION

Sound Pressure Measurements

A single ½" B&K microphone (model 4190, 1 *m* from the middle of the tunnel exit, under 45° to the center line) was used to measure the SPL (sampling rate: 25.6 *kHz*, Δf = 3.125 *Hz*) at the nozzle exit. Measurements were made with the empty muffler casing installed, the fully assembled muffler, and then the muffler with the small nozzle, each at the driving fan's max. operating conditions. Figure 4 (left) shows the results in comparison to the background noise level.

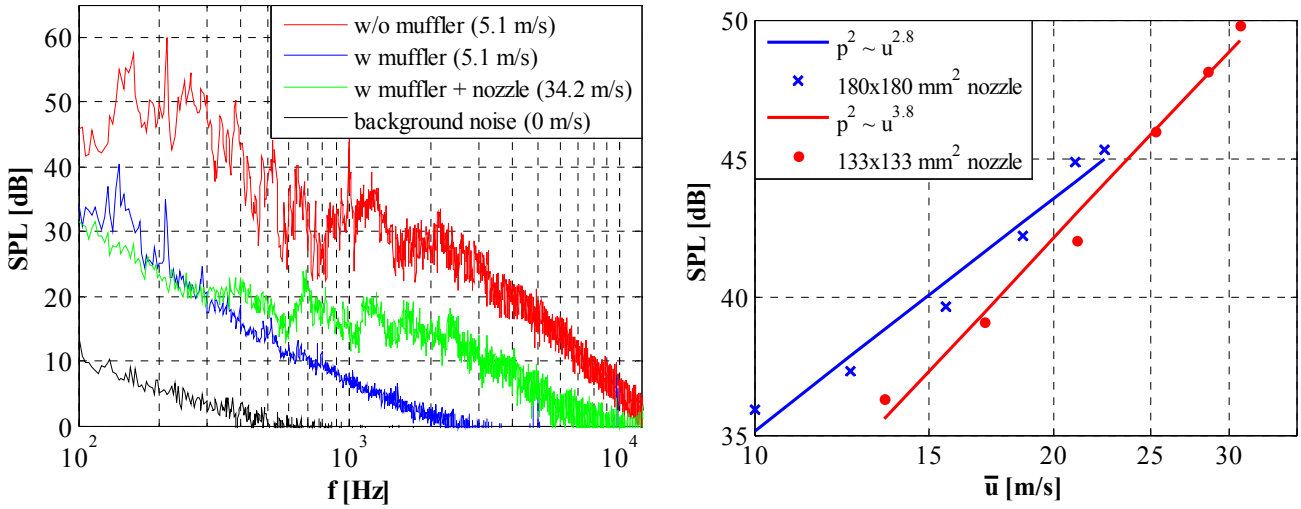

Figure 4: SPL (ref 20 μPa, Δf = 3.125 Hz) of the wind tunnel (left, for 133×133 mm^2 nozzle) and its scaling with velocity at the test section (right)

It is seen that the muffler reduces the SPL by 10-20 *dB* over the whole frequency range and also suppresses all higher harmonics of the blade passing frequency, except for the first one (~ 210 *Hz*). The SPL decreases for $f < 300$ *Hz* and increases for the remaining frequency range, when the nozzle is implemented. This increase is due to flow acceleration ($\bar{u} \approx 34.2$ *m/s*) and interaction with the nozzle lips. Figure 4 (right) shows the velocity scaling for the two nozzles implemented (measured with M2, see Figure 7, without airfoil installed). As is evident, a desired velocity $\bar{u} > 30$ *m/s* is achieved with the small nozzle. This indicates that the pressure losses have been correctly estimated in the design stage and the driving fan is correctly chosen.

Velocity Profiles and Turbulence Characteristics

The flow field has been measured with a standard a 1-D hotwire probe (DANTEC 55P11, sampling rate: 20 *kHz*), for both nozzle sizes and for three different velocities. Some example plots of mean and turbulent quantities for the larger nozzle are presented in Figure 5. The extent of the potential core of the jet is identifiable from both graphs: the turbulent mixing region is indicated by the increased level of turbulence intensity, as well as the decrease in the mean velocity. Profile non-uniformities, mainly at $x/D_0 = 0$, may arise from manufacturing inaccuracies of the nozzle. The bias could also be due to the influence of S-shaped bend on the flow, since the small nozzle shows quite similar velocity profiles. Overall, the minimum turbulence intensity is found to be around 0.4% in the middle of nozzle exit-plane and increases to levels of 5%-15% in the outer skirt of the potential core, where intense mixing occurs. For airfoil experiments, the streamwise location $x/D_0 = 0.56$ is important, since it marks the distance, where the airfoil leading edge will be located. At this distance, a turbulence intensity of around 0.36%-1% is present in the core region and the mean velocity profile is rather uniform as compared to the first plane.

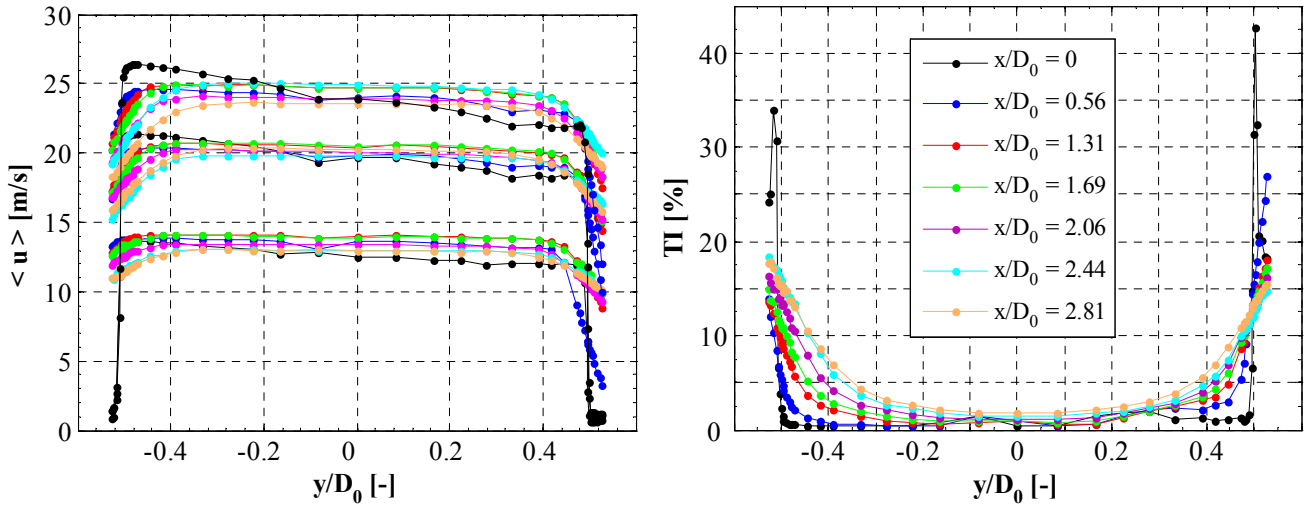

Figure 5: 180×180 mm² nozzle: Mean velocity profiles for three different free-stream velocities (left) and turbulence intensity profiles for max. free-stream velocity (right), both as functions of x

However, higher turbulence intensities are also observed in the jet core; a look at the energy spectrum reveals that the turbulence is anisotropic in the core-flow and isotropic towards the mixing region. To elaborate this, the 1-D turbulence energy spectrum is needed, which is defined as follows ([12], pp. 61-65):

$$E_x(f) = 4\left\langle u'^2 \right\rangle \int_0^\infty R_{xx}(\tau) e^{-j2\pi f\tau} d\tau = d\left\langle u'^2 \right\rangle / df \qquad (1)$$

It is often non-dimensionalized by

$$E_x(0) = 4\frac{\langle u'^2 \rangle}{\langle u \rangle}\Lambda_x \tag{2}$$

where u' is the fluctuating streamwise velocity component, R_{xx} is the streamwise autocorrelation function (i.e. the EULERIAN time correlation coefficient [12], p. 45). E_x is also referred to as the (one-sided) power spectral density function (in *dB/Hz*, e.g. estimated via WELCH's method, here obtained by the MATLAB® Vers. 7 routine *pwelch* [13] with a frequency resolution of Δf = 2.44 *Hz*) and Λ_x is the streamwise integral lengthscale. The latter one is obtained from the integral timescale Λ_t by assuming time delay and streamwise separation to be interchangeable, i.e. $\Lambda_x = \langle u \rangle \Lambda_t$ (TAYLOR's frozen turbulence hypothesis; e.g. [12], pp. 46-47). The integral timescale is determined from integrating the autocorrelation function up to the first zero-crossing ($\tau = t^*$), i.e.

$$\Lambda_t = \int_0^\infty R_{xx}(\tau)\,d\tau \approx \int_0^{t^*} \frac{\langle u'(t)u'(t+\tau)\rangle}{\langle u'(t)^2 \rangle}\,d\tau \tag{3}$$

Λ_x has also been calculated from the spectrum via Equation (2). Both methods led to almost identical results. The energy spectrum is compared to the VON KÁRMÁN spectrum [14] for isotropic turbulence, which reads (see also [15], pp. 696-701):

$$E_x(f) = \frac{E_x(0)}{\left[1+(k_x/k_e)^2\right]^{5/6}} \qquad with \qquad \frac{k_x}{k_e} = 2\sqrt{\pi}\,\frac{\Gamma(1/3)}{\Gamma(5/6)}\,\frac{f\Lambda_x}{\langle u \rangle} \tag{4}$$

A comparison of the obtained spectra and the autocorrelation functions for x/D_0 = 0.56 is given in Figure 6. As can be seen, the spectra agree very well for the lateral locations $y/D_0 > 0.45$, which substantiates the assumption that the nozzle flow is isotropic there. However, it is found that with the given sample rate (20 kHz) only the inertial subrange is resolved, with a typical KOLMOGOROV spectrum (-5/3 decay rate). The dissipation range, which exhibits exponential decay, is not resolved. Figure 6 shows that for a location far downstream in the mixing region and at lower velocities (data for big nozzle), this is different: for $f > 2$ *kHz*, the spectrum decays exponentially. A modified VON KÁRMÁN spectrum, which includes the exponential decay in the dissipation range, is obtained by multiplying Equation (4) with a non-dimensional function $f_\eta = e^{-\beta k_x/k_e}$ that tends to unity for small frequencies ([15], pp. 232-238). This approach yields an excellent curve-fit for β = 0.01 (see red line in Figure 6, indicated by the arrow). This is very similar to the value β = 0.015 obtained by MOREAU and ROGER [16, 17] for the wind tunnel facility at Ecole Centrale de Lyon. The TAYLOR microscale λ_x, which is calculated from the autocorrelation function and also from the energy spectrum, can lead to some conclusions, concerning the smallest possible scales in the flow (KOLMOGOROV scales). It can be calculated via one of the following two relations (see [12], p. 41):

$$\frac{1}{\lambda_x^2} = -\frac{1}{2\langle u \rangle^2}\left.\frac{\partial^2 R_{xx}}{\partial \tau^2}\right|_{\tau=0} \qquad or \qquad \frac{1}{\lambda_x^2} = \frac{2\pi^2}{\langle u \rangle^2 \langle u'^2 \rangle}\int_0^\infty E_x(f) f^2 df \tag{5}$$

Again, both methods yield very similar results (± 0.3 *mm*). Assuming isotropic turbulence, the microscale allows the calculation of the dissipation rate ε. From this, the KOLMOGOROV lengthscale is obtained by [12, 15]:

$$\eta = \left(\nu^3/\varepsilon\right)^{1/4} \qquad with \qquad \varepsilon = 30\nu\langle u'^2 \rangle / \lambda_x^2 \tag{6}$$

For the flow region, where isotropic behavior is observed, integral lengthscales decrease from $\Lambda_x \approx$ 7.0…5.1 *mm* with a respective microscale decrease of $\lambda_x \approx$ 2.8…1.4 *mm*, for locations y/D_0 = 0.45…0.53. The calculated KOLMOGOROV scales decrease from $\eta \approx$ 0.06…0.035 *mm*, leading to

highest possible frequencies of 18.4…34.6 *kHz*. Obviously, these scales cannot be resolved because of the limited sample rate. Correction of spectra and dissipation rate, by accounting for finite wire length [18], does not change the order of magnitude of the observations. In the anisotropic jet-core (cf. Figure 6, y/D_0 = 0.11), the integral lengthscale is around 30 *mm*, with $\lambda_x \approx 10$ *mm* and $\eta \approx 0.2$ *mm*, yielding a maximum frequency of around 27 *kHz*. The same anisotropic/ isotropic behavior is observed for different velocities, as well as for the big nozzle flow-field, with data points at $y/D_0 > 0.4$ showing isotropic behavior. The big nozzle at maximum velocity (≈ 24 *m/s*), provides integral lengthscales of $\Lambda_x \approx 8.5…7.2$ *mm* in the isotropic outskirt and around 20 *mm* in the jet-core. The principle observation is that the integral lengthscale decreases with increasing lateral distance y/D_0 from the center line, whereas the integral timescale increases (see Figure 6, right). It is worth to note that for all data points with isotropic turbulence, DRYDEN's [19] model autocorrelation function $R_{xx} = e^{-\tau/\Lambda_t}$ almost perfectly fits the measured autocorrelation function.

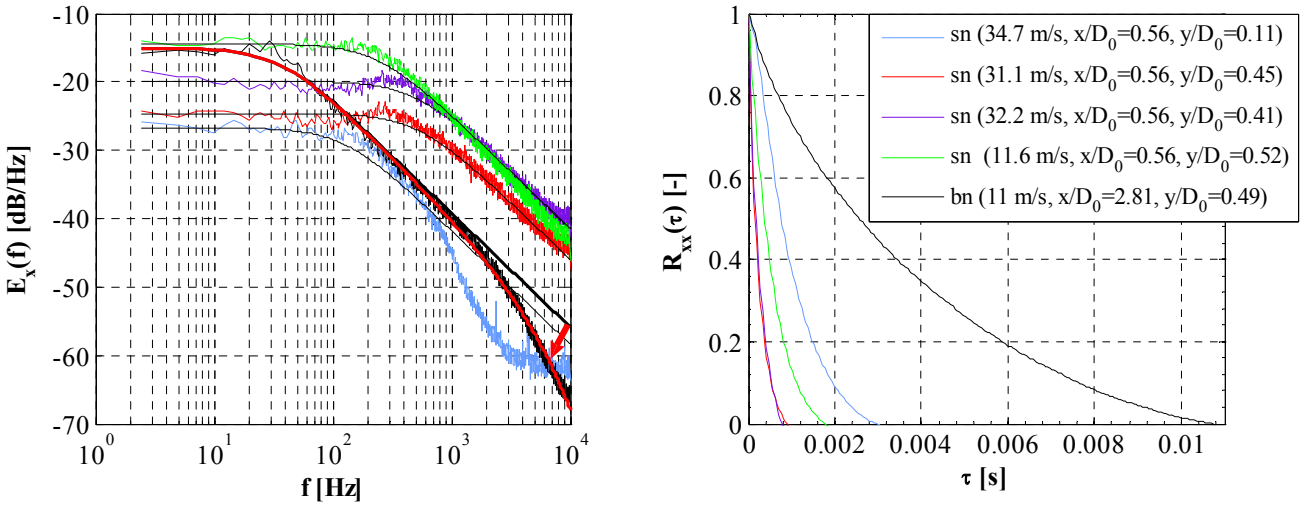

Figure 6: Turbulence energy spectra (left) compared to the VON KÁRMÁN spectrum (black lines) and autocorrelation functions (right) for sample points (bn = big nozzle, sn = small nozzle)

APPLICATION TO AIRFOIL MEASUREMENTS

Experimental Procedure

A NACA 6512-63 airfoil is mounted between two polycarbonate sideplates in front of the nozzle exit of the big nozzle, as depicted in Figure 7. The mock-up allows for angle-of-attack variations and its sideplates are flush mounted to the nozzle. The downstream edges of the sideplates are sharply bended away from the flow to avoid additional trailing edge noise. The airfoil has an aspect ratio of 1.33, a REYNOLDS number based on the chord length (c = 135 *mm*) of $Re_c \approx 2\times10^5$, and a leading edge distance to the nozzle exit-plane of 0.75c. Acoustic measurements are made with an arrangement of three ½" B&K model 4190 microphones. All microphones are placed at a distance of 120 *cm* from the trailing edge. M1 and M2 are on opposing sides under a right angle to the airfoil chord line, whereas M3 is mounted on a rotating arm, with a reference state of 30° to M2. The airfoil wake flow is surveyed by a single 1-D hotwire probe (TSI 1210-T1.5, sampling rate 20 *kHz*) mounted on a 3D-traverse system, which is controlled by a local PC. Results are presented in the following two sections.

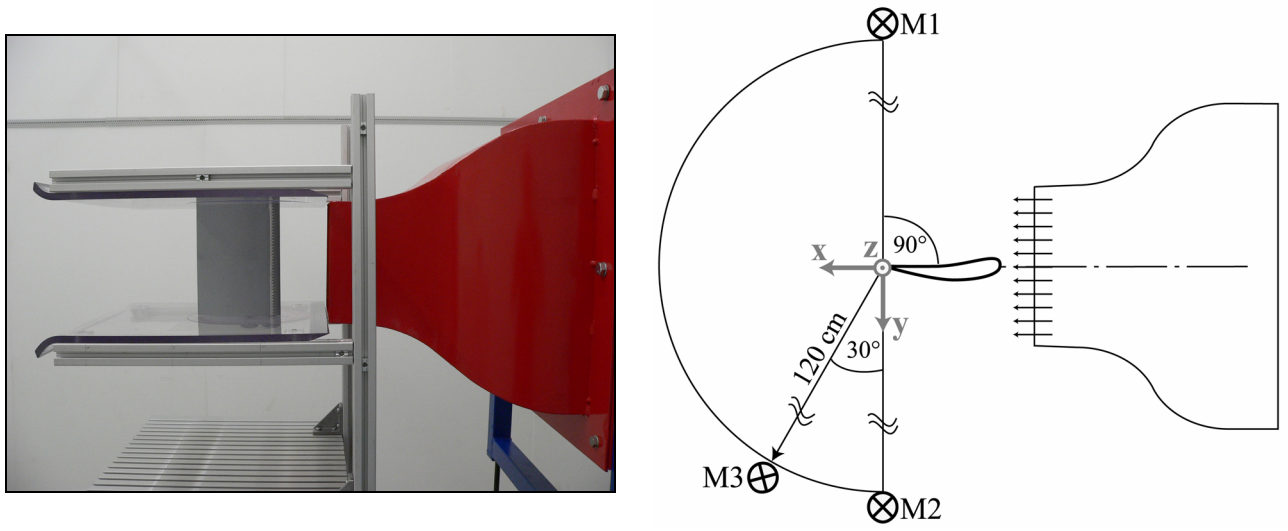

Figure 7: Airfoil mock-up and microphone arrangement for trailing edge noise measurements

Trailing Edge Noise Measurements

A critical issue in measuring the trailing edge noise is to distinguish it from other sound sources and from the facility background noise. In a first attempt, the signal of one microphone was used to obtain the SPL for the empty wind tunnel, for the mock-up installed in the wind tunnel, and for an airfoil installed in the mock-up. Figure 8 shows the SPL for these conditions. The frequency range where trailing edge noise is expected to occur (according to [20]) is indicated in the plot (left).

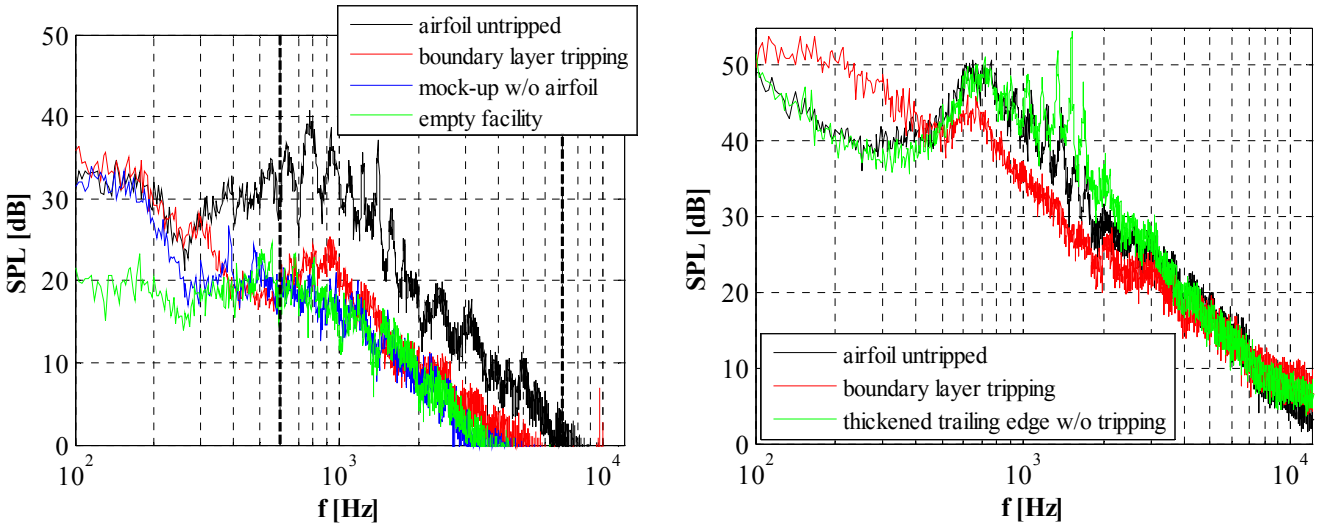

Figure 8: Left: SPL of M2 for different test arrangements with and without model airfoil and tripping (serrated tape). Right: SPL (40 cm from the trailing edge) of the airfoil with and without tripping (1.95 mm wire) and with an artificially thickened trailing edge (1.95 mm wire attached) without tripping

Figure 8 (left) shows a good signal-to-noise level for the desired frequency range. The recommended 10 *dB* difference to the background noise level in the usable range is mostly fulfilled. For this condition, the OASPL is found to scale with $u^{5.96}$, which is typical for a compact dipole source [21]. However, the spectrum exhibits numerous peaks in a zig-zag pattern, which are not expected and may be attributed to TOLLMIEN-SCHLICHTING instability waves in the laminar boundary layer on the airfoil [22], [23]. In order to obtain a fully turbulent boundary layer on both sides, the airfoil has been tripped by a serrated aluminum tape [24] of 290 μm nominal thickness and 5 *mm* width, on the pressure and suction side at 0.1*c*. As Figure 8 shows, the tripped airfoil results in much lower sound

emission, accompanied by a strong decrease in the signal-to-noise ratio. This leads to an almost unidentifiable trailing edge noise contribution, which has also been found by other investigators, cf. YU and JOSHI [25]. Accordingly, the signals from microphones M1 and M2 have been used for a correlation analysis to extract the noise that is radiated from the trailing edge of the tripped airfoil. The correlation and filtering technique of BLAKE and LYNCH [26] has been applied. It is assumed that trailing edge noise is of dipole character, with a phase of $\Theta_{12} = \pi$ between the signals reaching microphone M1 and M2 ([21], p. 490). Shear layer refraction effects [27] have been neglected in the analysis. In a first step, the cross-spectrum G_{12} between M1 and M2 is determined, with and without the airfoil installed in the mock-up. The spectra are compared, frequency by frequency. If the correlated airfoil noise for one frequency bin is less that 3 *dB* higher than the correlated background noise, this frequency bin is no longer considered to be assignable to trailing edge noise. For differences above 3 *dB*, the magnitude of the cross-spectrum background noise is subtracted from the magnitude of the cross-spectrum airfoil noise (which includes contributions from the airfoil *and* the facility background noise) for the frequency bin in consideration. With this, correlated background noise is eliminated and only correlated airfoil noise remains. For the frequency bins not rejected, the phase angle has been computed and if this value is in the range of $3/4\ \pi < |\Theta| < 5/4\ \pi$, it is assumed that the trailing edge noise mechanism with the known phase of π is the responsible source for this. Frequency bins outside this range are rejected. The result of this analysis in terms of the SPL is presented in Figure 9, for the tripped airfoil, and for comparison purposes, also for the untripped airfoil.

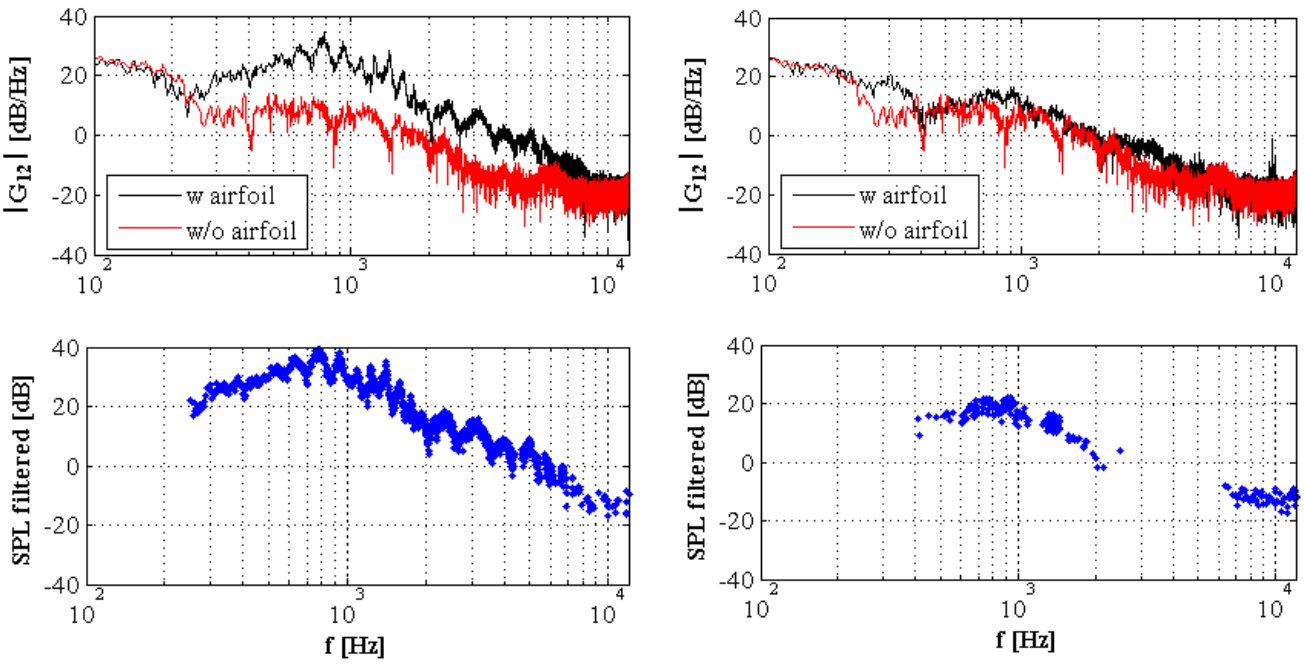

Figure 9: Trailing edge noise extraction technique for the untripped (left) and tripped (right) airfoil; top: Cross-spectra from M 1 and M2, bottom: Extracted trailing edge noise in SPL (Δf = 3.125 Hz)

It is worth noting that experiments with different tripping devices (sandpaper of different roughness, several layers of the serrated aluminum tape) lead qualitatively to the same result: the assigned trailing edge noise contribution is mostly concentrated in the region between 400 *Hz* and 2 *kHz*. A simple experiment shows that the peaks in the spectrum of the untripped airfoil are amplified (and slightly shifted) by artificial thickening of the trailing edge through attachment of a wire with $d_w \approx 12$ times the trailing edge thickness (Figure 8, right). This strong amplification stems from the trailing edge and is found to be in the range 800 *Hz* < *f* < 2.5 *kHz*. This frequency match substantiates that the filtered SPL in Figure 9 (right) is truly the contribution from the trailing edge. Figure 8 (right)

also shows that even though the peaks disappear, the tripping is suboptimal, since it raises the SPL over a wide frequency range, due to the wire dimensions. Overall, the serrated tape was found to be the best choice for boundary layer tripping, since it imposes the least disturbance to the flow.

Wake Flow Measurements

A wake survey has been performed to acquire knowledge on the mean and turbulent wake characteristics. The measurements are used to describe the reference flow conditions for future flow control experiments associated with momentumless wakes and turbulence control. Some preliminary results are presented in Figure 10.

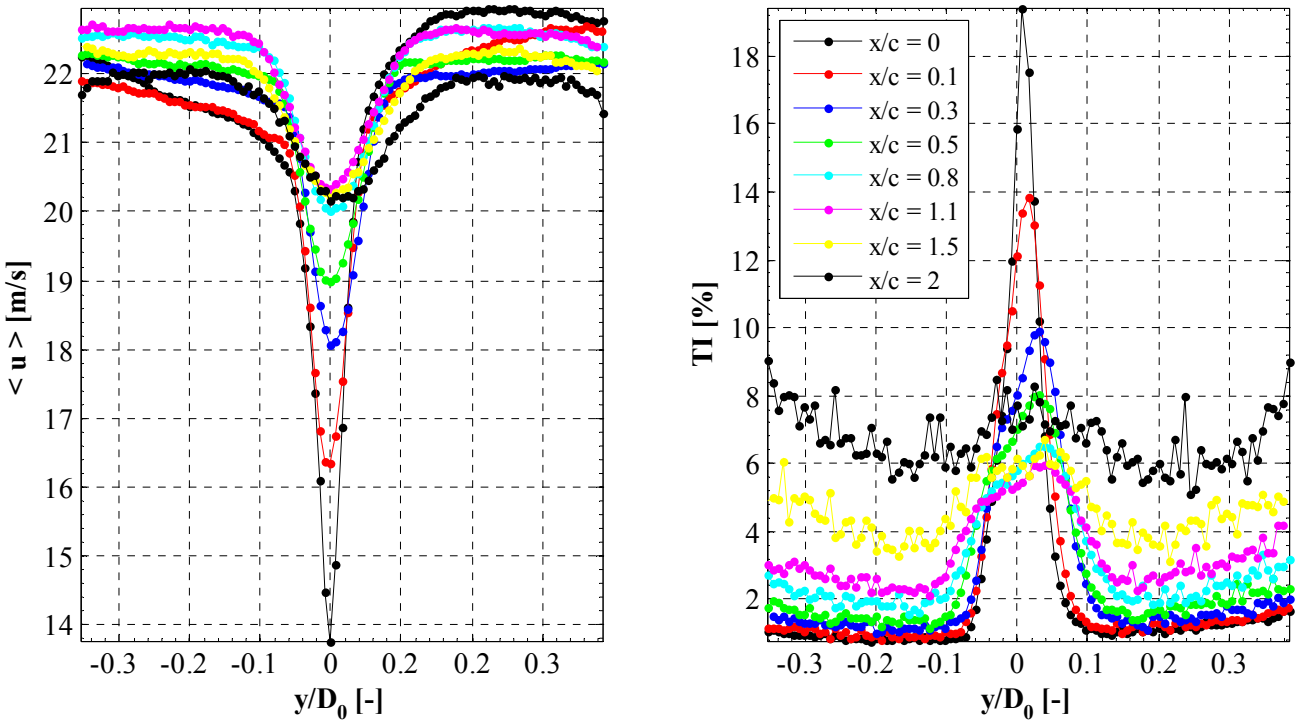

Figure 10: Mean and turbulent velocity profiles of the airfoil wake for different downstream locations from the trailing edge. Mean profile are measured from the wake center

Figure 10 (left) shows the decay of the mean velocity deficit with downstream distance ($\sim x^{-3.3}$). High mean velocity deficits are associated with high turbulent intensities, as evident from Figure 10 (right). The energy spectra reveal that turbulence is basically isotropic in the wake center region, with integral length scales continuously increasing from 3.6 *mm* to 60.2 *mm* at $x/c \approx 0$ and $x/c = 2$, respectively. The turbulence at $x/c = 1.5$ and 2 is important, since these downstream locations are representative for a typical fan stage rotor-stator spacing in jet engines. The turbulence structure is responsible for broadband noise production, due to unsteady loading on the stator vanes caused by the impingement of the rotor's turbulent blade-wakes. The high turbulence levels (4…8%), observed in Figure 10, are therefore indicative for potential broadband noise production. Nevertheless, the upwash turbulence spectrum (i.e. in *y*-direction) is required to assess the potential interaction-noise of the wake with a downstream stator vane [28]. This is part of an ongoing study.

CONCLUSIONS AND OUTLOOK

The aerodynamic and aeroacoustic performance of a new small wind tunnel was investigated. First measurements reported in this work indicate room for minor improvements concerning the flow

uniformity and turbulence. Basically, the nozzle contour or the design could be modified to achieve better overall flow uniformity. The latter seems to be most promising, since minor imperfections of the contour from the manufacture are indeed present and can have significant influence on the flow-field. A more sophisticated nozzle contour [11] may yield a better flow field. Also, the turbulence may be triggered by the contraction contour, since vortex stretching occurs in the accelerated flow field [29]. The desired $TI \approx 0.1\%$, as observed in other wind tunnels [2, 3], [30] could not be achieved, but comparable levels (< 0.8%) to other established test facilities [17], [20]. The lowest measured level was 0.36%. Further turbulence reduction is possible through a change in the screen-honeycomb combination, by (i) using a smaller cell-sized honeycomb, with a coarse screen placed at short distance upstream of it [31], with or without guiding vanes in the elbow pipes to support flow rectification; (ii) additional screens or changing the cascade by using a sequence of coarse to fine screens towards the nozzle [8]. In any case, a systematic study is required to evaluate the effectiveness of the suggested improvements. Nevertheless, the location where the airfoil is positioned shows a rather uniform velocity distribution and relatively low turbulence intensities (0.4%...1%). An additional silencer is not considered to be necessary, since most of the additional sound stems from the nozzle. Trailing edge noise measurements show that a correlation-filtering technique is required, as anticipated [26]. In future, fan blade sections will be investigated, with parameter variations to quantify and catalog the radiated sound.

ACKNOWLEDGEMENT

The airfoil-wake measurements had been carried out by Jean-Charles GBAGUIDI from Ecole Nationale Supérieure d'Arts et Métiers (ENSAM), Paris during his ERASMUS-stay at the University of Siegen. The authors would like to thank for this support.

BIBLIOGRAPHY

[1] G. SCHAUERTE, - *Konzeption und Auslegung eines kleinen aeroakustischen Windkanals*, Diplomarbeit Nr. A03-3/2 am Institut für Fluid- und Thermodynamik, Fachbereich Maschinenbau, Universität Siegen, pp. 81, **2004**

[2] T. J. MUELLER, D. F. SCHARPF, S. M. BATILL, R. B. STREBINGER, C. J. SULLIVAN, S. SUBRAMANIAN - *The Design of a Subsonic Low-Noise, Low-Turbulence Wind Tunnel for Acoustic Measurements*. Presented at AIAA 17th Aerospace Ground Testing Conference, Nashville, Tennessee, AIAA-1992-3883, **1992**

[3] T. J. MUELLER, D. A. LYNCH - *Chapter 5: An Anechoic Facility for Basic Aeroacoustic Research*. Aeroacoustic Measurements, T. J. Mueller (Ed.). Berlin: Springer, pp. 258-308, **2002**

[4] L. SCHMIDT, - *Akustische und aerodynamische Untersuchungen am neugebauten aeroakustischen Windkanal des Institutes für Technische Akustik*, Fakultät Elektrotechnik, Technische Universität Dresden, pp. 61, **1997**

[5] M. KRÄMER, X. ZHA, D. ECKOLDT, H. FUCHS - *Verbund-Platten-Resonator*, Offenlegungsschrift DE 102 13 107 A1, D. Patentamt, Fraunhofer-Gesellschaft zur Förderung der angewandten Forschung e.V., **2002**

[6] ISO: INTERNATIONAL ORGANIZATION FOR STANDARDIZATION - *ISO 3745:2003 - Determination of Sound Power Levels of Noise Sources Using Sound Pressure—Precision Methods for Anechoic and Hemi-Anechoic Rooms*, **2003**

[7] R. D. MEHTA, P. BRADSHAW - *Design Rules for Small Low Speed Wind Tunnels*, The Aeronautical Journal of the Royal Aeronautical Society, pp. 443-449, **1979**

[8] J. GROTH, A. V. JOHANSSON - *Turbulence Reduction by Screens*, Journal of Fluid Mechanics, vol. 197, pp. 139-155, **1988**

[9] R. I. LOEHRKE, H. M. NAGIB - *Control of Free-Stream Turbulence by Means of Honeycombs: A Balance Between Suppression and Generation*, Journal of Fluids Engineering, vol. 98, pp. 342-353, **1976**
[10] V. RAMJEE, A. K. M. F. HUSSAIN - *Influence of the Axisymmetric Contraction Ratio on Free-Stream Turbulence*, Journal of Fluids Engineering, vol. 98, pp. 506-515, **1976**
[11] Y.-X. SU - *Flow Analysis and Design of Three-Dimensional Wind Tunnel Contractions*, AIAA Journal, vol. 29, pp. 1912-1920, **1991**
[12] J. O. HINZE - *Turbulence*, 2nd ed., New York: McGraw-Hill Book Company, **1975**
[13] THE MATHWORKS INC. - *Matlab Version 7.3.0.267 R2006b*. Natick, Massachusetts: http://www.mathworks.com, **2006**
[14] T. VON KÁRMÁN - *Progress in the Statistical Theory of Turbulence*, Proceedings of the National Academy of Sciences of the United States of America, vol. 34, pp. 530-539, **1948**
[15] S. B. POPE - *Turbulent Flows*. Cambridge: Cambridge University Press, **2000**
[16] S. MOREAU, M. ROGER - *Competing Broadband Noise Mechanisms in Low-Speed Axial Fans*, AIAA Journal, vol. 45, pp. 48-57, **2007**
[17] S. MOREAU, D. NEAL, J. FOSS - *Hot-Wire Measurements Around a Controlled Diffusion Airfoil in an Open-Jet Anechoic Wind Tunnel*, Journal of Fluids Engineering, vol. 128, pp. 699-706, **2006**
[18] J. W. ELSNER, P. DOMAGALA, W. ELSNER - *Effect of Finite Spatial Resolution of Hot-Wire Anemometry on Measurements of Turbulence Energy Dissipation*, Measurement Science and Technology, vol. 4, pp. 517-523, **1993**
[19] H. L. DRYDEN, G. B. SCHUBAUER, W. C. J. MOCK, H. K. SKRAMSTAD - *Measurements of Intensity and Scale of Wind-Tunnel Turbulence and their Relation to the Critical Reynolds Number of Spheres*, NACA-TR-581, **1937**
[20] T. F. BROOKS, T. H. HODGSON - *Trailing Edge Noise Prediction from Measured Surface Pressures*, Journal of Sound and Vibration, vol. 78, pp. 69-117, **1981**
[21] W. K. BLAKE, J. L. GERSHFELD - *The Aeroacoustics of Trailing Edges*. Frontiers in Experimental Fluid Mechanics, M. Gad-el-Hak (Ed.). Berlin: Springer, pp. 457-532, **1989**
[22] C. K. W. TAM - *Discrete Tones of Isolated Airfoils*, The Journal of the Acoustical Society of America, vol. 55, pp. 1173-1177, **1974**
[23] E. C. NASH, M. V. LOWSON, A. MCALPINE - *Boundary-Layer Instability Noise on Aerofoils*, vol. 382, pp. 27-61, **1999**
[24] F. R. HAMA - *An Efficient Tripping Device*, Journal of the Aeronautical Sciences, vol. 24, pp. 236-237, **1957**
[25] J. C. YU, M. C. JOSHI - *On Sound Radiation from the Trailing Edge of an Isolated Airfoil in a Uniform Flow*. Presented at AIAA 5th Aeroacoustics Conference, Seattle, Washington, AIAA-1979-603, **1979**
[26] W. K. BLAKE, D. A. LYNCH - *Chapter 4: Source Characterization by Correlation Techniques*. Aeroacoustic Measurements, T. J. Mueller (Ed.). Berlin: Springer, pp. 218-257, **2002**
[27] R. K. AMIET - *Refraction of Sound by a Shear Layer*, Journal of Sound and Vibration, vol. 58, pp. 467-482, **1978**
[28] W. J. DEVENPORT, C. W. WENGER, S. A. L. GLEGG, J. A. MIRANDA - *Wave Number Frequency Spectra of a Lifting Wake for Broadband Noise Prediction*, AIAA Journal, vol. 36, pp. 881-887, **1998**
[29] M. L. BROWN, M. PARSHEH, C. K. AIDUN - *Turbulent Flow in a Converging Channel: Effect of Contraction and Return to Isotropy*, Journal of Fluid Mechanics, vol. 560, pp. 437-448, **2006**
[30] J. MATHEW, C. BAHR, B. CARROLL, M. SHEPLAK, L. CATTAFESTA - *Design, Fabrication, and Characterization of an Anechoic Wind Tunnel Facility*. Presented at 11th AIAA/CEAS Aeroacoustics Conference, Monterey, California, AIAA 2005-3052, **2005**
[31] C. FARELL, S. YOUSSEF - *Experiments on Turbulence Management Using Screens and Honeycombs*, Journal of Fluids Engineering, vol. 118, pp. 26-32, **1996**